Combined buoyant–thermocapillary flow in a cavity

By BRADLEY M. CARPENTER AND G. M. HOMSY

Department of Chemical Engineering, Stanford University, Stanford, CA 94305, USA

We treat the problem of combined buoyancy–thermocapillary convection in a cavity with a free surface heated differentially in the horizontal. Attention is focused on the structure and strength of the flow for large ΔT, i.e. large Marangoni and Rayleigh numbers. In the combined problem, the boundary-layer scalings for buoyant and thermocapillary convection suggest that in the limit of large ΔT, thermocapillarity will dominate the large-scale flow. Accurate numerical solutions are used to study this question at fixed cavity aspect ratio and Prandtl number, with $G = Ra/Ma$ as a parameter. For $G = 1$, the flow evolves toward its boundary-layer limit in a fashion identical to that for $G = 0$, i.e. pure thermocapillary flow. For $G = 10$, the evolution is from a buoyancy-dominated structure, through a transition, to a thermocapillary-dominated structure. We infer that thermocapillarity will ultimately dominate all such flows at sufficiently large ΔT, for any fixed values of G, the aspect ratio, and the Prandtl number.

1. Introduction

A non-uniform temperature field within a pure liquid bounded in part by a free surface produces two different sources of fluid motion, buoyancy and thermocapillarity. The flows associated with these two mechanisms considered independently have been extensively examined, the study of buoyancy-driven flow in cavities having an immense historical record. In this work we shall be concerned with the flow in a two-dimensional square cavity; buoyancy-driven flow in this geometry has been the subject of a comparison study to which over thirty groups contributed numerical solutions (de Vahl Davis & Jones 1983; de Vahl Davis 1983). The literature of thermocapillary flow is more recent and has been motivated primarily by the concerns of materials processing technology in microgravity. A numerical study important for its large parameter space is that of Fu & Ostrach (1983). The problem of the flow with combined mechanisms, however, has not been systematically investigated and is currently without a substantial theoretical basis, though preliminary numerical results by Bergman and coworkers (Bergman & Ramadhyani 1986; Bergman & Keller 1988) have established that thermocapillarity can be a significant influence in thermally driven cavity flows, particularly when thermocapillary stress acts to oppose the bulk circulation due to buoyancy. Experimental investigations of the combined flow have relied on dimensional estimates of the relative influence of the two mechanisms, estimates obtained by consideration of the parameters defining the flow: a fluid density ρ, a volumetric coefficient of thermal expansion β, gravity g, a length characteristic of the body L, the surface-tension thermal coefficient σ_T, a temperature difference ΔT, the dynamic viscosity μ, and the kinematic viscosity ν. Schwabe & Scharmann (1979) obtain the
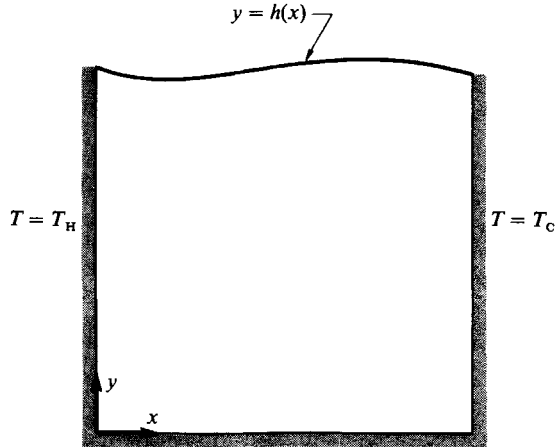
FIGURE 1. Thermally driven flow in a two-dimensional cavity. The upper surface is free and thermally insulated, the lower rigid and insulated.

group $\rho\beta g L^2/\sigma_T$ from a comparison of viscous scalings of thermocapillary and buoyancy effects. A characteristic 'thermocapillary velocity', U_{tc}, is obtained from the tangential stress balance, which requires $\mu U_{tc}/L \sim \sigma_T \Delta T/L$, and a "buoyancy velocity' U_b is given by the balance between viscous and buoyancy terms in the momentum equation, $\rho\beta g \Delta T \sim \mu U_b/L^2$. Schwabe & Scharmann's group then expresses the ratio U_b/U_{tc}. In this analysis, the lengthscale presumed appropriate to viscous stresses is L, the body lengthscale, and the analysis therefore cannot be valid in flows of boundary-layer character. Kamotani, Ostrach & Vargas (1984) use

$$\frac{\beta g L \mu^2}{\sigma_T^2 \Delta T} = \frac{\beta g \Delta T L^3}{\nu^2} \bigg/ \left(\frac{\sigma_T \Delta T L}{\mu\nu}\right)^2,$$

i.e. the Grashof number over the square of a surface-tension Reynolds number, to scale the influence of buoyancy to that of thermocapillarity. The group of Kamotani et al. represents the ratio of the square of a buoyancy velocity obtained by equating inertial terms in the momentum equation to the buoyancy term ($U_b^2/L \sim \beta g \Delta T$) to the square of the thermocapillary velocity obtained by Schwabe & Scharmann. The group of Schwabe & Sharmann suggests that buoyancy and thermocapillarity should be of comparable influence on Earth in fluid bodies having a characteristic length on the order of a centimeter, independent of the forcing thermal conditions; the scale of Kamotani et al. on the other hand, predicts that the influence of buoyancy will diminish relative to that of thermocapillarity as ΔT^{-1}. Though scaling estimates like those of Schwabe & Scharmann or Kamotani et al. may be adequate to characterize an experimentally observed flow, it is difficult to apply such estimates to convection-dominated flows with a high degree of confidence in the absence of a closer examination of the boundary-layer regime of the combined flow.

Our aim in this paper is to begin the development of a theoretical understanding of flow driven by the combined mechanisms of buoyancy and thermocapillarity for non-trivial Marangoni and Rayleigh numbers by examining a problem in which the boundary-layer structure of the flow due to each individually is well understood. This problem, sketched in figure 1, is the thermally driven flow in a fluid of Prandtl number of order unity in a square cavity with heated sidewalls. We consider a two-dimensional cavity of width L, filled to a height $y = L$ with a Boussinesq liquid. The

thermal conditions imposed on this cavity are: at $x = 0, T = T_H$; at $x = 1, T = T_C$; the upper and lower boundaries of the fluid are insulated. We take gravity to act in the $-y$ direction, and assume the contact lines of the free surface to be pinned on the vertical walls at $y = L$. Our problem is made dimensionless by reference to the following scaled variables:

$$x = \frac{x^*}{L}, \quad y = \frac{y^*}{L}, \quad T = \frac{T^* - T_H}{T_H - T_C}, \quad u, v = u^*, v^* \frac{\mu}{\Delta T \sigma_T}, \quad p = p^* \frac{\mu}{\sigma_T \nu L},$$

where the asterisked terms are dimensional variables.

Introduction of these quantities produces the following set of equations:

$$Re\,(uu_x + vu_y) = -p_x + \nabla^2 u, \quad Re\,(uv_x + vv_y) = GT - p_y + \nabla^2 v, \qquad (1\,a, b)$$

$$u_x + v_y = 0, \tag{2}$$

$$Ma\,(uT_x + vT_y) = \nabla^2 T, \tag{3}$$

$$u = v = 0, \quad T = 0 \quad (x = 0), \tag{4\,a, b, c}$$

$$u = v = 0, \quad T = -1 \quad (x = 1), \tag{5\,a, b, c}$$

$$u = v = 0, \quad T_y = 0 \quad (y = 0), \tag{6\,a, b, c}$$

$$\left.\begin{array}{c} v - uh_x = 0, \quad (T_y - T_x h_x)/N^{\frac{1}{2}} = 0, \\[4pt] -p + ((v_y - h_x u_y) + h_x(-v_x + h_x u_x))/N = Ca^{-1}h_{xx}(1 - Ca\,T)/N^{\frac{3}{2}}, \\[4pt] [(1 - h_x^2)(u_y + v_x) + 2h_x(v_y - u_x)]/N^{\frac{1}{2}} = -(T_x + T_y h_x), \\[4pt] N \equiv 1 + h_x^2, \end{array}\right\} \quad y = h(x) \qquad \begin{array}{c} (7\,a) \\[4pt] (7\,b) \\[4pt] (7\,c) \\[4pt] (7\,d) \end{array}$$

$$h(0) = h(1) = 1; \quad \int_{x=0}^{x=1} h(x')\,\mathrm{d}x' = 1. \tag{8\,a, b, c}$$

We have the Navier–Stokes equations (1), the continuity equation (2), the heat equation (3), and appropriate boundary conditions on the three rigid boundaries (4), (5), (6). On the free surface we have a kinematic condition (7a), an insulating thermal condition (7b), normal and tangential stress balances (7c) and (7d) respectively), and the additional requirements on h expressed in (8). The parameters in these equations are the Reynolds number, the Marangoni number, the capillary number, and a parameter reflecting the magnitude of the buoyant term relative to thermo-capillarity; they are defined as:

$$Re = \frac{(T_H - T_C)\,\sigma_T L}{\mu \nu}; \quad Ma = \frac{(T_H - T_C)\,\sigma_T L}{\mu \kappa} = Re\,Pr; \quad Ca = \frac{(T_H - T_C)\,\sigma_T}{\sigma_0}; \quad G = \frac{\beta g L^2}{\sigma_T}.$$

$$(9\,a\text{–}d)$$

In this work we shall assume that $Pr = 1$, so $Re = Ma$. The scale of buoyancy introduced here as G is identical to the parameter introduced by Schwabe & Scharmann (1979) to scale buoyancy effects. It is defined by them as a Bond number, but we have chosen an alternative name in order to avoid confusion with the many existing definitions of the Bond number. As noted previously, G describes the ratio of buoyant forces acting in the bulk to thermocapillarity acting on the free surface when the viscous lengthscale is L. The surface-tension Reynolds number and the Grashof number are related by $Gr = G\,Re$. The Marangoni and Rayleigh numbers are similarly related: $Ra = G\,Ma$.

With the assumption of vanishing capillary number, the location of the free surface has the simple solution $h = 1$, and the boundary conditions (7) simplify to

$$v_0 = 0, \quad T_{0y} = 0, \atop u_{0y} = -T_{0x}, \quad\Big\} \quad y = 1, \qquad (10a, b)$$

giving equations (1)–(6) and (10), the leading-order problem in a small-capillary-number expansion of the free-surface problem, as our system to be solved. For further discussion of this approximation, see Zebib, Homsy & Meiburg (1985).

2. Scaling considerations

The theory for buoyancy-driven flow in the boundary-layer regime in this situation is due to Gill (1966), which may be summarized for our purposes as follows. As Gr, the Grashof number ($\beta g \Delta T L^3 / \nu^2$), becomes large, flow in the cavity is driven by a temperature gradient of $O(\Delta T)$ across boundary layers adjacent to the hot and cold walls of the cavity. A balance of terms in these layers requires the layer thickness δ_b to be $O(L\,Gr^{-\frac{1}{4}})$ and the velocity U_b to be $O((\beta g \Delta T L^2 / \nu)\,Gr^{-\frac{1}{2}})$; the characteristic velocity therefore grows as $\Delta T^{\frac{1}{2}}$. Referred to the scales of equations (1)–(8), the dimensionless velocity scales with $G^{\frac{1}{2}}Re^{-\frac{1}{2}}$. In the central or core region of the cavity, the temperature depends only on the vertical coordinate, i.e. the isotherms are horizontally stratified, as are the streamlines of the core flow. As explained by Gill, this stratification is necessary to allow the buoyancy layers to both entrain and detrain fluid. From a knowledge of the scales for the thickness and velocity of the buoyancy layers, we may estimate the heat transfer in the cavity from the heat convected in the layers, proportional to $U_b \delta_b$. When velocities are scaled to $\beta g \Delta T L^2 / \nu$ and lengths to L, the dimensionless heat transfer across the cavity, or Nusselt number, of the buoyancy problem is proportional to $Gr^{\frac{1}{4}}$.

Thermocapillary flow in a square cavity has been studied numerically by Zebib *et al.* (1985), and by Carpenter & Homsy (1988). They find the flow at large Reynolds number ($\sigma_T \Delta T L / \mu\nu$) to be driven by an $O(\Delta T)$ temperature gradient along the free surface, a balance of terms in the surface layer then requiring that the characteristic velocity, U_{tc}, and the scale of the surface-layer thickness, δ_{tc}, satisfy $\mu U_{tc}/\delta_{tc} \sim \Delta T \sigma_T / L$, from the tangential stress balance, and $U_{tc}^2/L \sim \nu U_{tc}/\delta^2$, from the momentum equation. These two relations give the surface-layer thickness proportional to $L\,Re^{-\frac{1}{3}}$ and a characteristic velocity proportional to $(\sigma_T \Delta T/\mu)\,Re^{-\frac{1}{3}}$, yielding a characteristic velocity temperature dependence of $\Delta T^{\frac{2}{3}}$, or in the dimensionless variables of equations (1)–(8), the velocity is proportional to $Re^{-\frac{1}{3}}$. The Nusselt number of the thermocapillary problem, estimated from the heat convected in the surface layer as $Nu \sim Re\,Pr\,\delta U_{tc}\,T$, is proportional to $Re^{\frac{1}{3}}$.

Though the scalings of the thermocapillary and buoyancy layers are derived from purely local considerations, the scalings of the two layers cannot be simultaneously valid in a flow driven by the combined mechanisms, a consequence of the unequal orders of the two flows. The $O(Re^{-\frac{1}{3}})$ surface velocity of the thermocapillary flow creates a 'driven cavity pattern' of flow near the rigid walls of the cavity, i.e. $O(1)$ regions of separated flow in the two lower corners and in the upper left corner (adjacent to the hot wall), and $O(Re^{-\frac{1}{3}})$ boundary layers elsewhere on the walls. In the $O(Re^{-\frac{1}{3}})$ boundary layers adjacent to the vertical walls, the leading terms in the y-momentum equation are $O(Re^{\frac{2}{3}})$, while the buoyancy term is $O(1)$, given G fixed. If, therefore, thermocapillarity is sufficiently strong to establish an $O(Re^{-\frac{1}{3}})$ core flow,

the influence of buoyancy in these layers will be negligible in a first approximation. The question of which mechanism will dominate the flow in the cavity at large Reynolds number may be examined in the following way. If we consider a problem in which thermocapillarity is presumed to be weak, introducing the small parameter $\epsilon \equiv 1/G$, we rescale our equations to obtain

$$Gr\,(uv_x + vv_y) = T - p_y + \nabla^2 v, \tag{11}$$

$$Gr\,Pr\,(uT_x + vT_y) = \nabla^2 T, \tag{12}$$

$$u_{0y} = -\epsilon T_{0x}, \tag{13}$$

as y-momentum, heat, and tangential stress balances (the rest of (1)–(10) remaining unchanged). Seeking a solution for small ϵ of the form $\boldsymbol{u} = \boldsymbol{u}_0 + \epsilon \boldsymbol{u}_1 + O(\epsilon^2)$, the leading-order problem is simple buoyancy-driven flow, with $\boldsymbol{u}_0 \sim Gr^{-\frac{1}{2}}$. At $O(\epsilon)$ we require that the tangential stress balance be satisfied, and that inertial and viscous terms be of equal order in a layer of thickness δ near the free surface. These two requirements give with the result $\delta, \boldsymbol{u}_1 \sim Gr^{-\frac{1}{4}}$. The expansion for $\boldsymbol{u}$ is therefore $\boldsymbol{u} \sim Gr^{-\frac{1}{2}}\overline{\boldsymbol{u}_0} + \epsilon\,Gr^{-\frac{1}{4}}\overline{\boldsymbol{u}_1}$, the barred variables representing appropriately scaled $O(1)$ quantities. This expansion breaks down when $\epsilon \sim Gr^{-\frac{1}{4}}$. We may therefore expect the neglect of thermocapillarity to be invalid at sufficiently large Gr, with the consequence that the flow here cannot follow the scales of buoyancy-driven convection. When G is on the order of unity, buoyant and thermocapillary terms in (1b) and (10b) are of equal order. Under the assumption that the dimensionless free-surface temperature gradient remains $O(1)$ as $Re \to \infty$, the surface velocity (and hence the core velocities) must be $O(Re^{-\frac{1}{3}})$ in magnitude, with the result, as discussed previously, that the buoyancy term in the thermal boundary layers adjacent to the sidewalls is of $O(Re^{-\frac{1}{3}})$ relative to the leading terms in the boundary-layer momentum equation; buoyancy effects must therefore be negligible at large Reynolds number, a conclusion obviously also valid for small G. This leads to the surprising expectation that at large ΔT, the global structure of the flow will be that appropriate to the surface mechanism.

Our purpose, then, is to examine the thermally driven flow in a square cavity at large ΔT, and to describe the large-ΔT limit in the light of the preceding hypothesis. We will find that our numerical solutions uphold the hypothesis: under sufficiently large thermal driving forces, the character of the solutions with regard to core scaling and structure is essentially independent of the parameter G, i.e. the large-scale features of the flow tend toward the predictions of the thermocapillary theory as the influence of buoyancy is confined to thin regions near the vertical surfaces of the cavity.

3. Numerical solution

Numerical solution of this problem is made more convenient computationally by the introduction of a stream function Ψ $((u,v) = (\Psi_y, -\Psi_x))$, reducing the number of unknowns to two, Ψ and T. We apply conventional finite differencing to the equations for Ψ and T, approximating derivatives with centred differences in a consistent second-order-accurate manner. Our solution of the discrete equations follows the approach of Schreiber & Keller (1983), mixing Newton and chord steps to achieve computational economy. Parameter continuation is employed to obtain

	$y = 0.95$				
$x =$	0.07	0.17	0.52	0.87	0.95
Grid	Temperature				
64×64	0.143	0.00815	-0.0704	-0.0182	0.0254
74×74	0.143	0.00902	-0.0714	-0.0194	0.0240
84×84	0.137	0.00375	-0.0732	-0.0216	0.0208
Grid	Stream function				
64×64	-6.58×10^{-5}	-1.70×10^{-4}	-4.58×10^{-4}	-4.16×10^{-4}	-2.41×10^{-4}
74×74	-6.60×10^{-5}	-1.71×10^{-4}	-4.58×10^{-4}	-4.15×10^{-4}	-2.40×10^{-4}
84×84	-6.91×10^{-5}	-1.77×10^{-4}	-4.61×10^{-4}	-4.14×10^{-4}	-2.37×10^{-4}
	$x = 0.52$				
$y =$	0.07	0.17	0.52	0.87	0.95
Grid	Temperature				
64×64	-0.211	-0.0816	-0.0856	-0.0893	-0.0704
74×74	-0.211	-0.0821	-0.0873	-0.0910	-0.0714
84×84	-0.212	-0.0845	-0.0891	-0.0928	-0.0732
Grid	Stream function				
64×64	-1.48×10^{-4}	-6.27×10^{-4}	-1.67×10^{-3}	-9.36×10^{-4}	-4.58×10^{-4}
74×74	-1.51×10^{-4}	-6.39×10^{-4}	-1.67×10^{-3}	-9.37×10^{-4}	-4.58×10^{-4}
84×84	-1.48×10^{-4}	-6.27×10^{-4}	-1.68×10^{-3}	-9.44×10^{-4}	-4.61×10^{-4}

TABLE 1. Solution values at selected points as obtained on three different meshes, for the case $G = 0, Re = 1 \times 10^5$.

initial approximations to the solution at increasing Reynolds number; with this technique it is possible to advance the Reynolds number in increments ranging from 500 at $Re = 0$, to 5000 at $Re = 50000$, and obtain a converged solution (pointwise residual scaled to the solution less than 10^{-2}) in typically fewer than three Newton steps and twenty chord steps. Our results are obtained on 64×64 and 74×74 non-uniform meshes, giving systems of 7812 and 10512 equations. The meshes are graded toward the free surface and the vertical boundaries, with smallest spacings of approximately 0.006 in the upper corners of the cavity. As the thickness of the buoyancy layers as well as that of the surface layer is on the order of 0.1, the mesh spacing is small in comparison with dynamically important scales. The San Diego Supercomputer Center Cray X/MP-48 on which our work was performed required approximately three minutes of CPU time to compute an LU decomposition and fifteen seconds to complete a backsolve on the 74×74 system, using single precision LINPACK band mode routines modified to operate with out-of-core matrix storage, while retaining column pivoting. Representative data from a modest mesh refinement at $G = 0, Re = 1 \times 10^5$, from 64×64 to 84×84, given in table 1, show that the variation of the stream function and temperature at various points on the domain, relative to the maximum magnitudes of these variables, is generally less than 1%, i.e. the two solutions agree to within two significant figures, when significance is (appropriately) determined by the maximum magnitude of the variable within the domain. Some of the characteristics of our solutions at $G = 1$ and $G = 10$ are given in table 2. In this table $\Psi_{\min}$ is the minimum value of the stream function within the

			$G = 1$				
Re	Grid	$-\Psi_{\min}$	ω_{core}	$u(0.5, 1)$	Nu_{x-0}	Nu_{x-1}	$Nu_{x-0.5}$
5.0×10^3	64×64	3.84×10^{-3}	-8.92×10^{-2}	3.74×10^{-2}	3.57	3.54	3.54
10.0×10^3	64×64	3.26×10^{-3}	-6.73×10^{-2}	3.09×10^{-2}	3.39	3.36	3.35
20.0×10^3	74×74	2.94×10^{-3}	-5.74×10^{-2}	2.74×10^{-2}	5.57	5.63	5.50
30.0×10^3	74×74	2.94×10^{-3}	-5.74×10^{-2}	2.74×10^{-2}	6.30	6.36	6.25
40.0×10^3	74×74	2.94×10^{-3}	-5.74×10^{-2}	2.74×10^{-2}	6.85	6.93	6.84
50.0×10^3	74×74	2.94×10^{-3}	-5.74×10^{-2}	2.74×10^{-2}	7.29	7.40	7.33

			$G = 10$				
Re	Grid	$-\Psi_{\min}$	ω_{core}	$u(0.5, 1)$	Nu_{x-0}	Nu_{x-1}	$Nu_{x-0.5}$
4.0×10^3	64×64	3.71×10^{-3}	-5.47×10^{-2}	3.82×10^{-2}	4.14	4.17	4.15
5.0×10^3	64×64	3.29×10^{-3}	-4.97×10^{-2}	3.58×10^{-2}	4.51	4.51	4.40
6.0×10^3	64×64	3.00×10^{-3}	-4.05×10^{-2}	3.39×10^{-2}	4.63	4.68	4.64
8.0×10^3	64×64	2.61×10^{-3}	-3.28×10^{-2}	3.12×10^{-2}	5.00	5.07	5.02
10.0×10^3	74×74	2.46×10^{-3}	-3.35×10^{-2}	2.95×10^{-2}	5.46	5.45	5.33
14.0×10^3	74×74	2.49×10^{-3}	-3.79×10^{-2}	2.73×10^{-2}	6.01	5.98	5.86
20.0×10^3	74×74	2.42×10^{-3}	-3.94×10^{-2}	2.48×10^{-2}	6.66	6.61	6.50
30.0×10^3	74×74	2.26×10^{-3}	-3.66×10^{-2}	2.22×10^{-2}	7.45	7.40	7.30
40.0×10^3	74×74	2.12×10^{-3}	-3.42×10^{-2}	2.12×10^{-2}	8.06	8.01	7.92
50.0×10^3	74×74	2.02×10^{-3}	-3.22×10^{-2}	1.93×10^{-2}	8.56	8.52	8.44
60.0×10^3	74×74	1.93×10^{-3}	-3.07×10^{-2}	1.84×10^{-2}	8.98	8.96	8.88
70.0×10^3	74×74	1.85×10^{-3}	-2.94×10^{-2}	1.77×10^{-2}	9.35	9.34	9.28

TABLE 2. Characteristic quantities of some solutions at $G = 1$ and $G = 10$.

cavity, ω_{core} is the vorticity at the location of the minimum stream function, and Nu is the Nusselt number, the dimensionless heat flux across the cavity, calculated as

$$Nu(x) = \int_0^1 (Ma\, uT - T_x)\, dy.$$

This quantity, computed at $x = 0$ and at $x = 1$, shows an agreement generally better than 2 %.

4. Results

We first examine the behaviour of combined flow at $G = 1$. Our anticipated result here is that the influence of buoyancy will represent only a perturbation to the flow driven by thermocapillarity; this expectation is realized in the dependence of the minimum stream function on Reynolds number, shown in figure 2. The lower curve in this figure, the result for $G = 0$, shows the expected $Re^{-\frac{1}{3}}$ dependence to within about 5%. At large Reynolds number, the difference between the two curves essentially vanishes; near $Re = 5 \times 10^4$, the minimum stream function of the $G = 1$ solution is proportional to $Re^{-0.31}$, and is equal to the $G = 0$ value to within two significant figures.

The structural features of the large-Reynolds-number flow and temperature fields at $G = 1$ also correspond closely with the $G = 0$ solutions. Figure 3 shows the stream function and temperature contours at $Re = 3.5 \times 10^4$ for $G = 0$ and $G = 1$. In both of these solutions, the qualitative features associated with the establishment of the
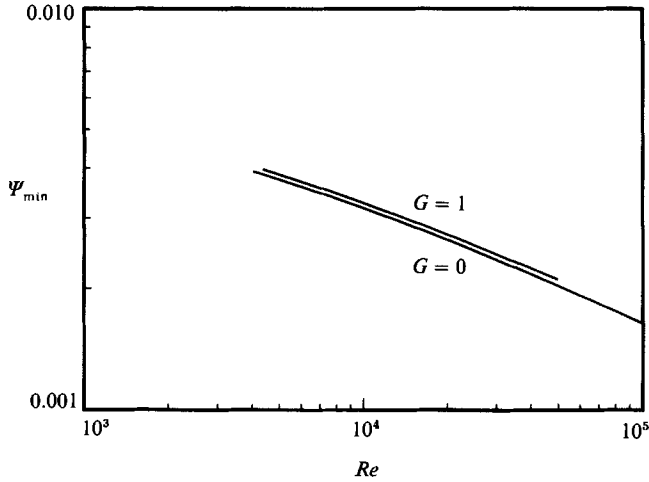
FIGURE 2. Scaling behaviour of the minimum stream function with Reynolds number.

closed streamline, constant-vorticity core region of large-Reynolds-number thermo-capillary flow are apparent. A secondary vortex is present in the lower right corner of the cavity in the $G = 1$ solution, clearly an effect of the adverse pressure gradient created by the core flow on the lower part of the cold wall. Buoyancy retains some influence locally, as evidenced by the suppression of separation on the bottom wall near the hot boundary. The third region of separated flow, in the upper left corner, is not yet developed at this Reynolds number in either the $G = 0$ or the $G = 1$ solution. The temperature distribution at $G = 1$ also differs little from the pure thermocapillary result. Temperature gradients are confined to the boundaries of the cavity; the core region is nearly isothermal, as is appropriate for convection-dominated transport in a region of closed streamlines.

The instance $G = 10$ (or $\epsilon = 0.1$, in the scaling of (10)–(13)) describes a situation in which the buoyancy-driven flow, if considered independent of thermocapillarity, should begin to display boundary-layer characteristics at $Re = Gr/G \sim 1 \times 10^3$, when $\delta_b \sim \frac{1}{10}L$. If, however, the scaling analysis of the combined buoyancy and thermocapillary problem presented in the previous section is valid, we might expect the flow to show significant departure from the pattern of buoyancy-driven convection at $Re \approx 1 \times 10^3$, since $Gr^{-\frac{1}{4}} \approx \epsilon$.

Our numerical solutions at a value of G equal to 10 show that, with regard to the scaling behaviour of the minimum stream function, the flow is dominated by buoyancy to a Reynolds number of approximately 1×10^4. Near this value it undergoes the abrupt change of character seen in figure 4. In figure 4, the upper curve is the minimum stream function for $G = 0$. In a range from $Re = 4 \times 10^3$ to $Re = 8 \times 10^3$, the minimum stream function is proportional to $Re^{-0.51}$, in close agreement with the prediction of classical buoyancy-driven boundary-layer theory. Beyond $Re = 1 \times 10^4$, the flow enters a brief transitional regime in which Ψ_{min} is nearly independent of Re, and then begins to approach the $G = 0$ scaling. Near $Re = 6 \times 10^4$, $\Psi_{min} \sim Re^{-0.30}$. It is interesting to note that though buoyancy and thermocapillarity both act to produce a clockwise circulation in the cavity, their effects are not additive and, at the Reynolds numbers we have examined, the combined flow is significantly weaker than the pure thermocapillary flow. This can be attributed to the influence of buoyant convection on the free-surface temperature gradient, which, as can be
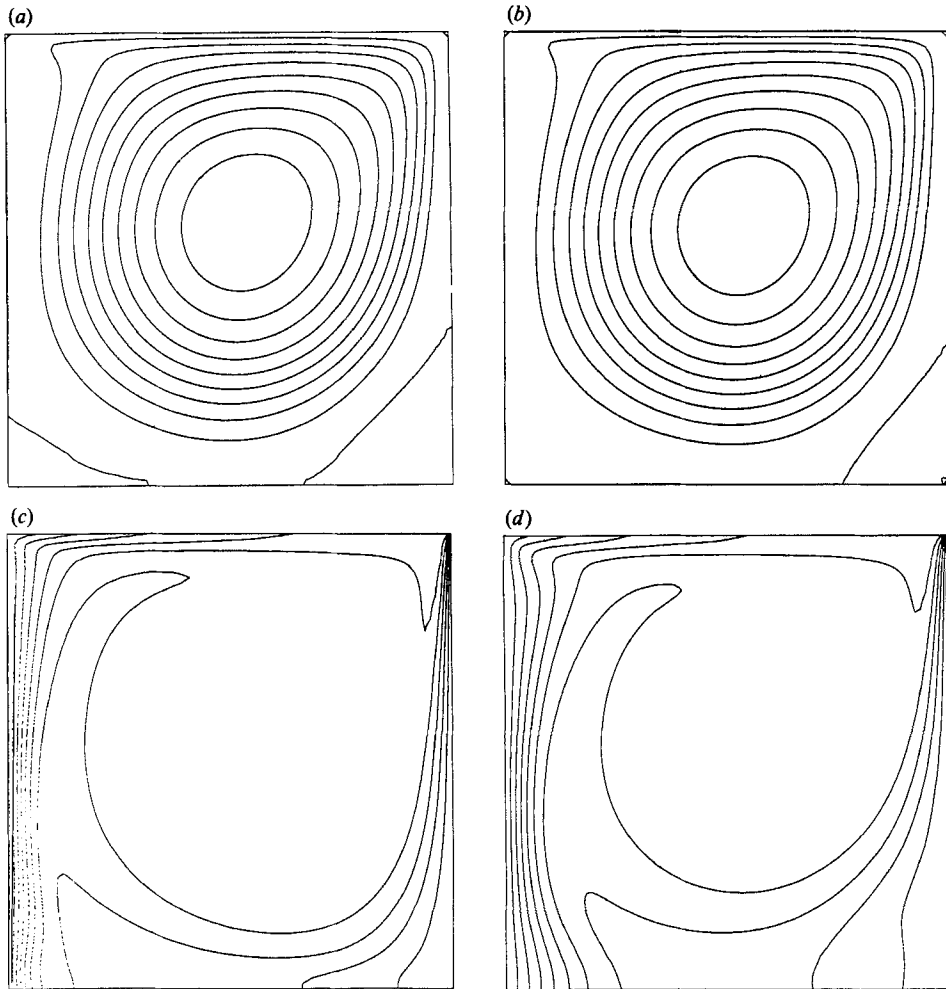
FIGURE 3. Stream function and temperature contours for $G = 0$ and $G = 1$ solutions at $Re = 3.5 \times 10^4$: (a) stream function, $G = 0$; (b) stream function, $G = 1$; (c) temperature, $G = 0$; (d) temperature, $G = 1$.

seen in figure 5, is somewhat smaller over the central region of the free surface (away from the boundaries) at $G = 10$ than at $G = 0$, for $Re = 1 \times 10^4$. The surface temperature gradient at $x = 0.5$ on these curves has a value of -0.34 for $G = 0$; at $G = 10$ the gradient diminishes to -0.24. The fact that the dimensionless temperature gradient over the central region of the free surface at large Reynolds number is actually approximately -0.24, not the value of -1 assumed in the scaling arguments of the previous section, explains why the transition to thermocapillary dominance appears slightly later than the scaling analysis predicts – the effective thermocapillary stress is only one quarter of the assumed value over the dynamically significant portion of the free surface.

The evolution toward thermocapillary patterns on increasing Re can also be seen qualitatively in the contours presented in figure 6, which presents solutions at $Re = 5 \times 10^3$ and at $Re = 7 \times 10^4$. Near $Re = 5 \times 10^3$, in the interval over which the minimum stream function scales close to the prediction of the buoyancy theory, the
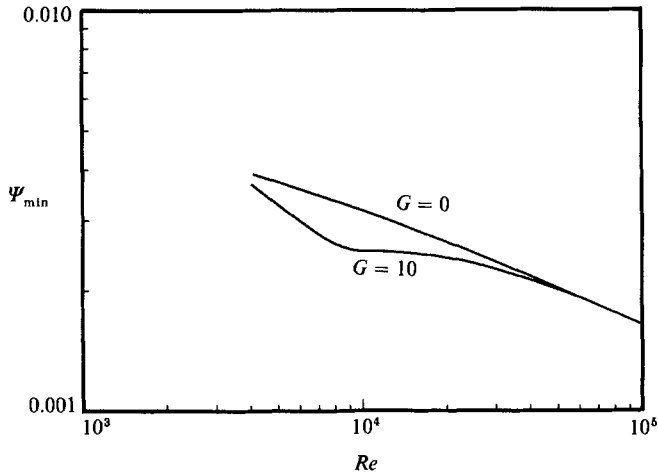
FIGURE 4. Scaling behaviour of the minimum stream function with Reynolds number for $G = 10$ and $G = 0$.
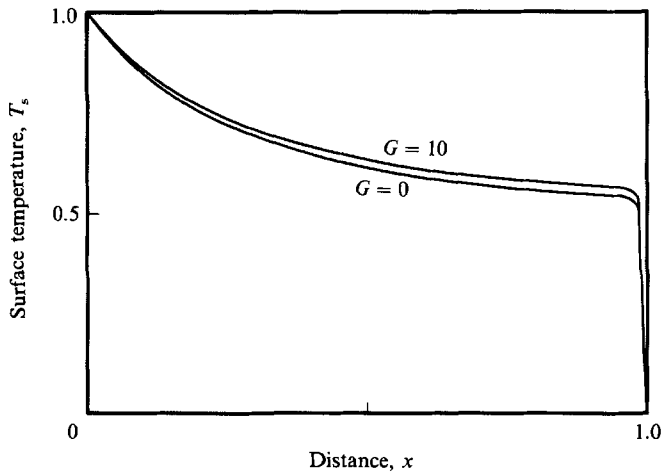
FIGURE 5. Surface temperature distributions at $Re = 10^4$ for $G = 10$ and $G = 0$.

streamlines and temperature contours of the core region show horizontal strati-fication in correspondence with the theoretical description of Gill. At $Re = 7 \times 10^4$, the core patterns are distinctly thermocapillary in origin, with a nearly isothermal temperature distribution and the circular streamlines of a constant-vorticity core flow. The influence of buoyancy at $Re = 7 \times 10^4$ is principally manifested in the suppression of the secondary vortices in the lower corners of the cavity. Buoyancy provides an acceleration to the flow in the vicinity of the cold wall which counteracts the adverse pressure gradient represented by the decelerating core flow, and so stabilizes the boundary layer on the lower half of the cold wall. Buoyancy cannot act similarly on the lower horizontal boundary, and a small region of separated flow therefore appears. Buoyant acceleration prevents the separating streamline from reattaching on the hot wall. These effects are Reynolds-number-dependent, and we would expect the flow to acquire a structure completely analogous to the pure thermocapillary problem at sufficiently large Reynolds number.
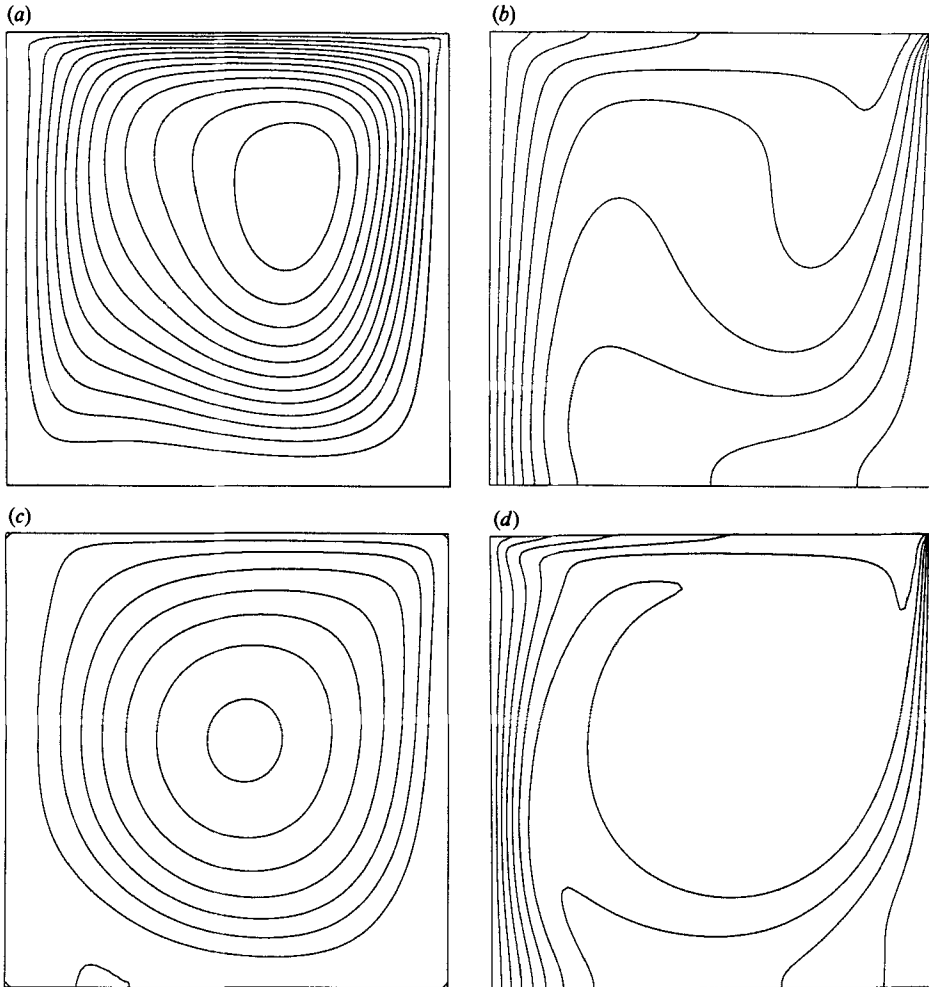
FIGURE 6. Stream function and temperature contours for $G = 10$. $Re = 5 \times 10^3$: (*a*) stream function, (*b*) temperature. $Re = 7 \times 10^4$: (*c*) stream function, (*d*) temperature.

5. Discussion

This paper is a limited investigation of combined thermocapillary and buoyancy-driven flow. The combined flow problem will have a parametric dependence on many factors about which it is impossible to draw quantitative conclusions, but some qualitative extensions are possible. We have seen how thermocapillarity eventually dominates the flow at sufficiently large Reynolds number for $Pr = 1$, $G = 1$ or 10, and how this can be explained by the weaker Reynolds-number-dependence of thermocapillary flows, which are $O(Re^{-\frac{1}{3}})$ at high Reynolds number, while buoyancy-driven flow is $O(Re^{-\frac{1}{2}})$. Our explanation implies that thermocapillarity will dominate the flow at any fixed value of G or Pr, if the Reynolds number is large enough, as the scaling dependencies remain asymptotically valid. The same conclusion, surprisingly, would be true of the cavity aspect ratio: no matter how small the area of the free surface, the flow field in the core of the cavity must be $O(Re^{-\frac{1}{3}})$ at asymptotically large Reynolds numbers.

REFERENCES

CARPENTER, B. M. & HOMSY, G. M. 1988 High Marangoni number convection in a square cavity, part 2. *Phys. Fluids* (submitted).

FU, B. I. & OSTRACH, S. 1983 In *Proc. ASME Winter Meeting, Boston, Massachusetts, November 13–18, 1983*. ASME.

GILL, A. E. 1966 *J. Fluid Mech.* **26**, 515.

KAMOTANI, Y., OSTRACH, S. & VARGAS, M. 1984 *J. Cryst. Growth* **66**, 83.

SCHREIBER, R. & KELLER, H. B. 1983 *J. Comput. Phys.* **49**, 310.

SCHWABE, D. & SCHARMANN, A. 1979 *J. Cryst. Growth* **46**, 125.

VAHL DAVIS, G. DE 1983 *Intl J. Num. Meth. Fluids* **3**, 249.

VAHL DAVIS, G. DE & JONES, I. P. 1983 *Intl J. Num. Meth. Fluids* **3**, 227.

ZEBIB, A., HOMSY, G. M. & MEIBURG, E. 1985 *Phys. Fluids* **28**, 3467.